PCCP

COMMUNICATION

View Article Online
View Journal | View Issue

Cite this: *Phys. Chem. Chem. Phys.*, 2023, **25**, 19422

Received 12th June 2023,
Accepted 6th July 2023

DOI: 10.1039/d3cp02733c

rsc.li/pccp

The treatment of dispersion terms for solution systems†

De-Cai Fang, * Si-Cong Liu, Dan-Yang Liu and Xin-Rui Zhu

DFT calculations of reaction mechanisms in solution have always been a hot topic, especially for transition-metal-catalyzed reactions, in which the traditional DFT-D3 method has been extensively employed. The overestimation of the dispersion from the traditional DFT-D3 method leads to a quite low activation free-energy barrier, so it is worth finding a proper way to deal with the dispersion for solution systems. The solvent–solute dispersion is also important for solution systems, and thus it should be calculated together with the solute dispersion. The newly generated solute–solute dispersion energy should be shared equally with the newly formed cavity between two interacting species; therefore, only half of the solute–solute and solvent–solute dispersion terms belong to the solute molecule. The detailed treatment of dispersion correction for solution systems has been fully addressed, and this method has been confirmed with the examples of ligand exchange reactions and catalytic reactions.

The molecular Schrödinger equation for the solution systems is quite complex because the noncovalent interactions between solute and solvent molecules become evident.[1] To simplify the calculation for the solutional systems, the general approach is to consider the solutional potential as a perturbation term $\hat{V}_{\text{int}}$ of the solute research system, as shown in eqn (1):

$$\hat{H} = \hat{H}^0 + \hat{V}_{\text{int}} \tag{1}$$

In general, solvation energy generated from solute–solvent interaction operator $\hat{V}_{\text{int}}$ consists of electrostatic energy operator $\hat{V}_{\text{es}}$ and non-electrostatic energy operator $\hat{V}_{\text{non-es}}$.[2–4] The electrostatic energy is generated from the permanent dipole conducted by an induction force, and non-electrostatic energy usually refers to dispersion energy, cavitation energy and repulsion energy, where the solvent–solute dispersion energy is originated from the transient dipole between solute and solvent molecules.

In fact, the total energy for solution systems can be written as:

$$E = \langle \Psi | \hat{H}^0 + \frac{1}{2}\hat{V}_{\text{int}} | \Psi \rangle \tag{2}$$

where $\hat{H}^0$ is the Hamilton operator *in vacuo*, $|\Psi\rangle$ is the wave function, and $\hat{V}_{\text{int}}$ is the solute–solvent interaction operator. Factor $\frac{1}{2}$ is defined as the decrease in the interaction energy due to solvent polarization work,[5–7] in other words, a solute molecule and its cavity should reach a thermal equilibrium. Therefore, a solute molecule holds only half of the solvent–solute interaction energy. The solvent–solute electrostatic interaction operator has been put into Hamilton operator $\hat{H}^{\text{s}}$, namely:

$$\hat{H}^{\text{s}} = \hat{H}^0 + \frac{1}{2}\hat{V}_{\text{es}} \tag{3}$$

and the corresponding energy is calculated as:

$$E^{\text{s}} = E^0 + \frac{1}{2}E_{\text{es}} \tag{4}$$

This is really an equation for the Polarizable continuum model (PCM)[8–11] in modern quantum programs, since the Tomasi group[12] suggested that the dispersion energy and cavitation energy might cancel each other out.

London dispersion interaction, which is a long-range attractive force, originates from the temporary dipole moment of molecules.[13–16] This weak interaction is particularly important in large or condensed systems such as biological systems and nanomaterials.[17] However, the description of London dispersion interaction is missing in density functional theory (DFT) due to its inaccurate electron correlation expression by empirical parameters.[18]

The dispersion operator $\hat{V}_{\text{D}}$ can be put into $\hat{H}^{\text{s}}$ for solute molecules, namely,

$$\hat{H}^{\text{s}}_{\text{D}} = \hat{H}^0 + \hat{V}_{\text{D}} + \frac{1}{2}\hat{V}_{\text{es}} \tag{5}$$

College of Chemistry, Beijing Normal University, Beijing 100875, P. R. China. E-mail: dcfang@bnu.edu.cn

† Electronic supplementary information (ESI) available: Computational results and discussion. See DOI: https://doi.org/10.1039/d3cp02733c

and the corresponding energy for a solute molecule in solution can be expressed as:

$$E_{\mathrm{D}}^{\mathrm{s}} = E^{0} + E_{\mathrm{D}} + \frac{1}{2}E_{\mathrm{es}} \tag{6}$$

Herein, E_{D} is estimated with dispersion corrected density functional theory (DFT-D3),[19] although the dispersion energy E_{D} is a constant for a fixed geometry in general. Eqn (5) and (6) are usually employed by most researchers for DFT-D3 and PCM calculations.

The solvent–solute dispersion energy E_{SSD} from its operator $\hat{V}_{\mathrm{SSD}}$ should also be considered due to the concurrent solute dispersion E_D and solvent–solute dispersion, the latter of which is originated from eqn (2). Therefore, the Hamilton operator $\hat{H}_{\mathrm{D}}^{\mathrm{s}}$ and its energy become:

$$\hat{H}_{\mathrm{D}}^{\mathrm{s}} = \hat{H}^{0} + \hat{V}_{\mathrm{D}} + \frac{1}{2}\hat{V}_{\mathrm{es}} + \frac{1}{2}\hat{V}_{\mathrm{SSD}} \tag{7}$$

and

$$E_{\mathrm{D}}^{\mathrm{s}} = E^{0} + E_{\mathrm{D}} + \frac{1}{2}E_{\mathrm{es}} + \frac{1}{2}E_{\mathrm{SSD}} \tag{8}$$

Herein, the solvation energy $\Delta E_{\mathrm{D}}^{\mathrm{s}}$ is calculated as:

$$\Delta E_{\mathrm{D}}^{\mathrm{s}} = \frac{1}{2}E_{\mathrm{es}} + \frac{1}{2}E_{\mathrm{SSD}} \tag{9}$$

Now we will test eqn (9) by using of data sets from Truhlar's group,[20] which was developed for a solvation model with state-specific polarizability (SMSSP) based on SMD. The calculation of solvent–solute dispersion E_{SSD} is based on the work of Tomasi and coworkers,[21,22] which has been adapted into the Gaussian program.[23] Herein, one should note that modern quantum programs deal with the E_{es} term in eqn (9) correctly, but the Gaussian program calculates the E_{SSD} term without the factor of $\frac{1}{2}$.[24] In fact, only half of the solvent–solute dispersion energy E_{SSD} belongs to the solute molecule, as indicated in eqn (9).

The comparison for 621 solvation energy data sets is shown in Fig. 1, which shows that the Mean-Square-Deviation (RMSD) value is 1.32 and 90% of the data is within the range of ± 2. This indicates that eqn (9) is good enough for calculating the solvation energy.

For the process of A + B → A···B in solution, there is solvent–solute dispersion (in black ovals), solute dispersion (in blue ovals) and solute–solute dispersion (in red oval, ΔE_{D} (A···B)), as indicated in Fig. 2. The solute–solute dispersion ΔE_{D} (A···B) is newly generated when the A molecule approaches the B molecule, in which the partial cavities of A and B molecules are destroyed and a new cavity of A···B is formed, as indicated in the interaction region of Fig. 2. Therefore, only half of the solute–solute dispersion ΔE_{D} (A···B) belongs to the solute molecule, in order to establish a new thermal equilibrium between the A···B solute molecule and the newly formed cavity (black curves in Fig. 2). In other words, the total dispersion interaction operator $\hat{V}_{\mathrm{D}}^{\mathrm{s}}$(A···B) and the corresponding energy $E_{\mathrm{D}}^{\mathrm{s}}$(A···B) can be expressed as:

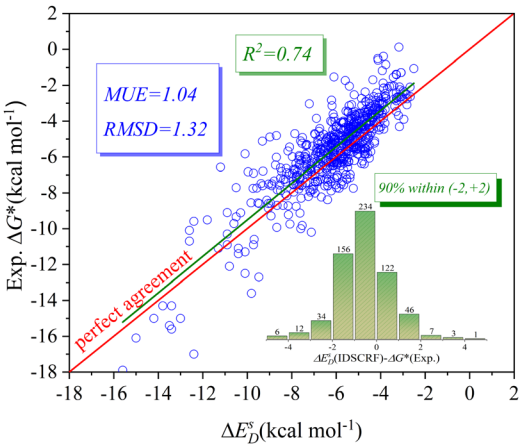

Fig. 1 The comparison of the calculated solvation energy data with experimental solvation data, and the inset is the histogram of $\Delta E_{\mathrm{D}}^{\mathrm{s}}$ (IDSCRF)-ΔG^{*} (Exp) for 621 datasets.

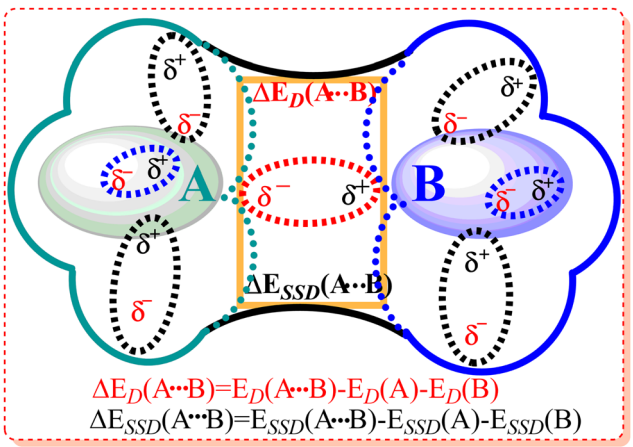

Fig. 2 The subsystem of solute and cavity that describes the solvent–solute dispersion (in black ovals), the solute dispersion (in blue ovals), along with the newly formed solute–solute dispersion (ΔE_{D}(A···B), in red ovals) and solvent–solute dispersion (ΔE_{SSD} in the interaction region between A and B molecules).

$$\hat{V}_{\mathrm{D}}^{\mathrm{s}}(\mathrm{A}\cdots\mathrm{B}) = \hat{V}_{\mathrm{D}}(\mathrm{A}) + \hat{V}_{\mathrm{D}}(\mathrm{B}) + \frac{1}{2}\Delta\hat{V}_{\mathrm{D}}(\mathrm{A}\cdots\mathrm{B}) + \frac{1}{2}\hat{V}_{\mathrm{SSD}}(\mathrm{A}) + \frac{1}{2}\hat{V}_{\mathrm{SSD}}(\mathrm{B}) + \frac{1}{2}\Delta\hat{V}_{\mathrm{SSD}}(\mathrm{A}\cdots\mathrm{B}) \tag{10}$$

and

$$E_{\mathrm{D}}^{\mathrm{s}}(\mathrm{A}\cdots\mathrm{B}) = E_{\mathrm{D}}(\mathrm{A}) + E_{\mathrm{D}}(\mathrm{B}) + \frac{1}{2}\Delta E_{\mathrm{D}}(\mathrm{A}\cdots\mathrm{B}) + \frac{1}{2}E_{\mathrm{SSD}}(\mathrm{A}) + \frac{1}{2}E_{\mathrm{SSD}}(B) + \frac{1}{2}\Delta E_{\mathrm{SSD}}(\mathrm{A}\cdots\mathrm{B}) \tag{11}$$

Therefore, the contribution of dispersion to the relative energy $\Delta E_{\mathrm{D}}^{\mathrm{s}}$(A···B) in solution is counted as:

$$\Delta E_{\mathrm{D}}^{\mathrm{s}}(\mathrm{A}\cdots\mathrm{B}) = \frac{1}{2}\Delta E_{\mathrm{D}}(\mathrm{A}\cdots\mathrm{B}) + \frac{1}{2}\Delta E_{\mathrm{SSD}}(\mathrm{A}\cdots\mathrm{B}) \tag{12}$$

Table 1 Comparison of experimental ΔH data with those from various calculation methods for 12 selected reactions (in kcal mol^{-1})

Reaction[a]	ΔH_{exp}[a]	ΔH_{cal}[b]	ΔH_{cal}[c]	ΔH_{cal}[d]	$\frac{1}{2}\Delta E_D$	$\frac{1}{2}\Delta E_{SSD}$
1ab	12.0	14.4	−1.2	9.9	−7.8	3.3
1ac	8.2	13.6	−11.4	8.0	−12.5	6.9
1bc	−3.8	−0.8	−10.2	−2.8	−4.7	2.7
2ab	15.5	17.5	−5.5	10.7	−11.5	4.7
3ab	14.1	22.5	−8.9	13.1	−15.7	6.3
1a	−38.9	−28.2	−42.6	−33.9	−7.2	1.5
1b	−26.9	−13.8	−42.8	−24.0	−14.5	4.3
1c	−30.7	−14.6	−54.6	−25.8	−20.0	8.8
2a	−38.4	−28.2	−42.6	−33.9	−7.2	1.5
2b	−22.9	−11.2	−42.6	−21.3	−15.7	5.6
3a	−32.2	−23.2	−32.5	−27.1	−4.6	0.8
3b	−18.1	−0.8	−41.5	−14.0	−20.3	7.2
RMSD		10.3	16.7	3.6		

[a] Ref. 25, and see Scheme S1 in ESI for detailed reaction equations. [b] B3LYP+IDSCRF/TZP-DKH(-dfg), eqn (4). [c] B3LYP-D3+IDSCRF/TZP-DKH(-dfg), eqn (6). [d] B3LYP-D3a+IDSCRF/TZP-DKH(-dfg), eqn (12).

This is really an equation for calculating the dispersion contribution to relative energies for A + B → A···B reaction. Afterwards, we will employ DFT calculations on some reaction processes for testing eqn (12), which includes the ligand exchange reactions, and the transition metal catalytic reactions.

Jacosen and Cavallo[25] said that "When phosphanes of different sizes are compared, functionals including dispersion interactions, at odds with experimental evidence, predict that larger phosphanes bind more strongly than smaller phosphanes, while functionals not including dispersion interaction reproduce the experimental trends with reasonable accuracy". In fact, this is not the case, since the treatment of the dispersion term in solution with eqn (6) is not very appropriate.

The calculated data, along with experimental measurements, are listed in Table 1, from which one can observe that B3LYP-PCM/TZP-DKH(-dfg) with our IDSCRF radii[26] (B3LYP+IDSCRF/TZP-DKH(-dfg)) are predicted to be more positive than those from the experimental enthalpy change[25] for all reactions (*c.f.* columns 3 and 2). Jacobsen and Cavallo[25] have employed different DFT methods without dispersion to calculate these data, and have drawn a similar conclusion. This indicates that the dispersion correction is important for such ligand exchange reactions. However, B3LYP-D3+IDSCRF/TZP-DKH(-dfg) (column 4, eqn (6)) provides more negative reaction enthalpies for all reactions, which are even qualitatively inconsistent with experimental measurements for the first 5 reactions (*c.f.* columns 4 and 2). The data from B3LYP-D3a+IDSCRF/TZP-DKH(-dfg) (column 5) are calculated with eqn (12), which are much better than those from the other two methods (*cf.* RMSD values of columns 3,4 and 5 in Table 1). The values of $\frac{1}{2}\Delta E_D$ (A···B) and $\frac{1}{2}\Delta E_{SSD}$ (A···B) in eqn (12) are also listed in Table 1, from which one can observe that the solute–solute dispersion favors larger phosphane binding, but the solvent–solute dispersion has the reverse effect.

We have chosen eleven experimentally well-investigated catalytic reactions as our testing subjects, which include four Ru-catalytic C–H activation/cycloadditions (**M1**–**M4**),[27–30] two Ru-catalytic C–H activation/C–C couplings (**M5**, **M6**),[31,32] two Rh-catalytic reactions (**M7**, **M8**),[33,34] and three Pd-catalytic reactions (**M9**, **M10** and **M11**).[35–37] We have published the reaction mechanisms for some of the reactions in the same or similar methods, for example, **M1**,[38] **M6**[39] and **M7**.[40] We have also redone some reactions, *e.g.*, **M3**,[41] **M5**,[42] **M10**[43] and **M11**[44] with the present method.

In order to test the present method, one needs to calculate the entropy in solution correctly, for which our solution-phase translational entropy model, coded in the THERMO program,[45] has been employed. The cavity volume (V_{cav}) and molecule volume (V_{mol}) can be estimated by the overlapping spheres[46] with our IDSCRF radii[26] and Bader's radii,[47,48] respectively, and the detailed methodology is described in our recent perspective paper.[24]

Table 2 lists the estimated activation free-barriers ΔG_{est} and the calculated values ΔG_{cal}, the latter of which are based on the TOF-determining transition state (TDTS) and intermediate (TDI) of the energy span model.[49–51] It can be observed from Table 2 that B3LYP-D3+IDSCRF/TZP-DKH(-dfg) (column 5, eqn (6)) provides quite low activation free-energy barriers for all reactions (except **M7**). The largest error reaches 15.6 kcal mol^{-1} for reaction **M3**, and the RMSD is *ca.* 9.1. B3LYP+IDSCRF/TZP-DKH(-dfg) (column 6, eqn (6)) calculates quite high activation free-energy barriers for all reactions, indicating that the dispersion correction is important for characterizing such reactions. It can be seen that the largest error is 17.2 kcal mol^{-1} for reaction **M7**, and the RMSD is *ca.* 6.0 (see column 6). Therefore, the best calculation method is B3LYP-D3a+IDSCRF/TZP-DKH(-dfg) (column 4, eqn (12)), since RMSD is only 1.9.

In conclusion, DFT investigation has currently been widely applied to study the reaction mechanisms in solutional systems, in which the dispersion correction is crucial for most systems. The traditional treatment of the dispersion is not proper for the solution systems, since it overestimates the

Table 2 The estimated activation free-energy barriers, along with the calculated data (kcal mol^{-1}) for the selected catalytic reactions

Reaction[a]	Temp. (K)	Time (h)	$\Delta G^{\ddagger}_{est}$[b]	$\Delta G^{\ddagger}_{cal}$[c]	$\Delta G^{\ddagger}_{cal}$[d]	$\Delta G^{\ddagger}_{cal}$[e]
M1	358	10	28.5	28.5	16.6	32.9
M2	443	24	36.0	34.7	24.7[f]	39.1[f]
M3	333	2	25.5	22.2	9.9	26.2
M4	363	12	29.1	29.6	17.1	35.0
M5	333	24	27.0	24.7	16.5	27.8
M6	373	24	30.5	28.2	19.7	35.7
M7	384	0.2	28.0	31.5	31.0[f]	45.2
M8	343	15	27.5	26.4	22.2	27.4
M9	298	6–72	25.0	25.8	20.0	26.9
M10	298	24	24.2	24.1	21.6	25.3
M11	373	36	30.6	32.0	24.4	31.1
RMSD				1.9	9.1	6.0

[a] See Scheme S2 in the ESI for the reaction schemes. [b] Estimated from experimental temperature and time. [c] B3LYP-D3a+IDSCRF/TZP-DKH(-dfg), eqn (12). [d] B3LYP-D3+IDSCRF/TZP-DKH(-dfg), eqn (6). [e] B3LYP+IDSCRF/TZP-DKH(-dfg), eqn (4). [f] TDI and/or TDTS at different structures.

solute–solute dispersion. The proper way is to consider the correction of our present eqn (12), in which only half of the solute–solute dispersion ΔE_{D} (A$\cdots$B) and solvent–solute dispersion ΔE_{SSD} (A$\cdots$B) belong to the solute molecule.

Author contributions

De-Cai Fang: designing and writing the whole manuscript, and calculating the data in Table 1. Si-Cong Liu, Dan-Yang Liu and Xin-Rui Zhu: calculating the reaction mechanisms and free-energy data in Table 2.

Conflicts of interest

There are no conflicts to declare.

Acknowledgements

The authors are thankful for financial support from the National Nature Science Foundation of China (22173010).

Notes and references

1 E. V. Anslyn and D. A. Dougherty, *Mordern Physical Organic Chemistry*, University Science Books, the United States of America, 2005.
2 A. Ben-Naim, *Water and Aqueous Solutions*, Springer, New York, NY, New York, 1st edn, 1974.
3 A. Ben-Naim, Standard thermodynamics of transfer. Uses and misuses, *J. Phys. Chem.*, 1978, **82**, 792–803.
4 A. Ben-Naim, *Solvation Thermodynamics*, Springer, New York, NY, New York, 1st edn, 1987.
5 J. Tomasi and M. Persico, Molecular Interactions in Solution: An Overview of Methods Based on Continuous Distributions of the Solvent, *Chem. Rev.*, 1994, **94**, 2027–2094.
6 A. A. Rashin and B. Honig, Reevaluation of the Born model of ion hydration, *J. Phys. Chem.*, 1985, **89**, 5588–5593.
7 J. M. Herbert, Dielectric continuum methods for quantum chemistry, *Wiley Interdiscip. Rev.: Comput. Mol. Sci.*, 2021, **11**, e1519.
8 S. Miertuš, E. Scrocco and J. Tomasi, Electrostatic interaction of a solute with a continuum. A direct utilizaion of AB initio molecular potentials for the prevision of solvent effects, *Chem. Phys.*, 1981, **55**, 117–129.
9 G. Schüürmann, M. Cossi, V. Barone and J. Tomasi, Prediction of the pK_a of Carboxylic Acids Using the ab Initio Continuum-Solvation Model PCM-UAHF, *J. Phys. Chem. A*, 1998, **102**, 6706–6712.
10 J. Tomasi, R. Cammi, B. Mennucci, C. Cappelli and S. Corni, Molecular properties in solution described with a continuum solvation model, *Phys. Chem. Chem. Phys.*, 2002, **4**, 5697–5712.
11 J. Tomasi, R. Cammi and B. Mennucci, Medium effects on the properties of chemical systems: An overview of recent formulations in the polarizable continuum model (PCM), *Int. J. Quantum Chem.*, 1999, **75**, 783–803.
12 M. Cossi, V. Barone, R. Cammi and J. Tomasi, Ab initio study of solvated molecules: a new implementation of the polarizable continuum model, *Chem. Phys. Lett.*, 1996, **255**, 327–335.
13 A. J. Stone, *The Theory of Intermolecular Forces*, Oxford University Press, Oxford, 2nd edn, 2013.
14 J. E. Jones and S. Chapman, On the determination of molecular fields.- I. From the variation of the viscosity of a gas with temperature, *Proc. R. Soc. London, Ser. A*, 1924, **106**, 441–462.
15 J. E. Jones and S. Chapman, On the determination of molecular fields. - II. From the equation of state of a gas, *Proc. R. Soc. London, Ser. A*, 1924, **106**, 463–477.
16 J. E. Jones and S. Chapman, On the determination of molecular fields. III. - From crystal measurements and kinetic theory data, *Proc. R. Soc. London, Ser. A*, 1924, **106**, 709–718.
17 S. Grimme, A. Hansen, J. G. Brandenburg and C. Bannwarth, Dispersion-Corrected Mean-Field Electronic Structure Methods, *Chem. Rev.*, 2016, **116**, 5105–5154.
18 W. Koch and M. C. Holthausen, *A Chemist's Guide to Density Functional Theory*, John Wiley, Sons, New York, 2nd edn, 2015.
19 S. Grimme, J. Antony, S. Ehrlich and H. Krieg, A consistent and accurate ab initio parametrization of density functional dispersion correction (DFT-D) for the 94 elements H-Pu, *J. Chem. Phys.*, 2010, **132**, 154104.
20 A. V. Marenich, C. J. Cramer and D. G. Truhlar, Uniform Treatment of Solute-Solvent Dispersion in the Ground and Excited Electronic States of the Solute Based on a Solvation Model with State-Specific Polarizability, *J. Chem. Theory Comput.*, 2013, **9**, 3649–3659.
21 F. Floris and J. Tomasi, Evaluation of the dispersion contribution to the solvation energy. A simple computational model in the continuum approximation, *J. Comput. Chem.*, 1989, **10**, 616–627.
22 F. M. Floris, J. Tomasi and J. L. P. Ahuir, Dispersion and repulsion contributions to the solvation energy: Refinements to a simple computational model in the continuum approximation, *J. Comput. Chem.*, 1991, **12**, 784–791.
23 M. J. Frisch, G. W. Trucks, H. B. Schlegel, G. E. Scuseria, M. A. Robb, J. R. Cheeseman, G. Scalmani, V. Barone, B. Mennucci, G. A. Petersson, H. Nakatsuji, M. Caricato, X. Li, H. P. Hratchian, A. F. Izmaylov, J. Bloino, G. Zheng, J. L. Sonnenberg, M. Hada, M. Ehara, K. Toyota, R. Fukuda, J. Hasegawa, M. Ishida, T. Nakajima, Y. Honda, O. Kitao, H. Nakai, T. Vreven, J. A. J. Montgomery, J. E. Peralta, F. Ogliaro, M. Bearpark, J. J. Heyd, E. Brothers, K. N. Kudin, V. N. Staroverov, R. Kobayashi, J. Normand, K. Raghavachari, A. Rendell, J. C. Burant, S. S. Iyengar, J. Tomasi, M. Cossi, N. Rega, J. M. Millam, M. Klene, J. E. Knox, J. B. Cross, V. Bakken, C. Adamo, J. Jaramillo, R. Gomperts, R. E. Stratmann, O. Yazyev, A. J. Austin, R. Cammi, C. Pomelli, J. W. Ochterski, R. L. Martin, K. Morokuma, V. G. Zakrzewski, G. A. Voth, P. Salvador,

J. J. Dannenberg, S. Dapprich, A. D. Daniels, O. Farkas, J. B. Foresman, J. V. Ortiz, J. Cioslowski and D. J. Fox, *Gaussian 09, Revision A.02*, Gaussian, Inc., Wallingford, CT, 2009.

24 S.-C. Liu, X.-R. Zhu, D.-Y. Liu and D.-C. Fang, DFT calculations in solution systems: solvation energy, dispersion energy and entropy, *Phys. Chem. Chem. Phys.*, 2023, **25**, 913–931.

25 H. Jacobsen and L. Cavallo, On the Accuracy of DFT Methods in Reproducing Ligand Substitution Energies for Transition Metal Complexes in Solution: The Role of Dispersive Interactions, *ChemPhysChem*, 2012, **13**, 562–569.

26 J.-Y. Tao, W.-H. Mu, G. A. Chass, T.-H. Tang and D.-C. Fang, Balancing the atomic waistline: Isodensity-based scrf radii for main-group elements and transition metals, *Int. J. Quantum Chem.*, 2013, **113**, 975–984.

27 P. P. Kaishap, G. Duarah, B. Sarma, D. Chetia and S. Gogoi, Ruthenium(II)-Catalyzed Synthesis of Spirobenzofuranones by a Decarbonylative Annulation Reaction, *Angew. Chem., Int. Ed.*, 2018, **57**, 456–460.

28 H. Miura, S. Terajima and T. Shishido, Carboxylate-Directed Addition of Aromatic C–H Bond to Aromatic Aldehydes under Ruthenium Catalysis, *ACS Catal.*, 2018, **8**, 6246–6254.

29 X. Wu, B. Wang, S. Zhou, Y. Zhou and H. Liu, Ruthenium-Catalyzed Redox-Neutral [4+1] Annulation of Benzamides and Propargyl Alcohols *via* C–H Bond Activation, *ACS Catal.*, 2017, **7**, 2494–2499.

30 J. Wang, X. Zhang, J. Zhou, L. Yan, Y. Li, N. Zhao, H. Liu, H. Huang and Y. Zhou, A Ru(II)-catalyzed C–H activation and annulation cascade for the construction of highly coumarin-fused benzo[*a*]quinolizin-4-ones and pyridin-2-ones, *Org. Chem. Front.*, 2023, **10**, 2680–2687.

31 X.-Q. Hu, Z. Hu, G. Zhang, N. Sivendran and L. J. Gooßen, Catalytic C–N and C–H Bond Activation: ortho-Allylation of Benzoic Acids with Allyl Amines, *Org. Lett.*, 2018, **20**, 4337–4340.

32 P. Keshri, K. R. Bettadapur, V. Lanke and K. R. Prabhu, Ru(II)-catalyzed C–H activation: amide-directed 1,4-addition of the ortho C–H bond to maleimides, *J. Org. Chem.*, 2016, **81**, 6056–6065.

33 Y. Ohta, S. Yasuda, Y. Yokogawa, K. Kurokawa and C. Mukai, Stereospecific and Stereoselective Rhodium(I)-Catalyzed Intramolecular [2+2+2] Cycloaddition of Allene-Ene-Ynes: Construction of Bicyclo [4.1.0] heptenes, *Angew. Chem., Int. Ed.*, 2015, **54**, 1240–1244.

34 S. E. Korkis, D. J. Burns and H. W. Lam, Rhodium-catalyzed oxidative C–H allylation of benzamides with 1, 3-dienes by allyl-to-allyl 1, 4-Rh(III) migration, *J. Am. Chem. Soc.*, 2016, **138**, 12252–12257.

35 C. F. Rosewall, P. A. Sibbald, D. V. Liskin and F. E. Michael, Palladium-catalyzed carboamination of alkenes promoted by N-fluorobenzenesulfonimide *via* C–H activation of arenes, *J. Am. Chem. Soc.*, 2009, **131**, 9488–9489.

36 Z. Wang, Y. Kuninobu and M. Kanai, Palladium-Catalyzed Oxirane-Opening Reaction with Arenes *via* C–H Bond Activation, *J. Am. Chem. Soc.*, 2015, **137**, 6140–6143.

37 X. Wang, Y. Lu, H.-X. Dai and J.-Q. Yu, Pd(II)-Catalyzed Hydroxyl-Directed C–H Activation/C–O Cyclization: Expedient Construction of Dihydrobenzofurans, *J. Am. Chem. Soc.*, 2010, **132**, 12203–12205.

38 H.-J. Long, L. Zhang, B. Lian and D.-C. Fang, DFT study on ruthenium-catalyzed decarbonylative annulation of an alkyne with six-membered hydroxychromone *via* C–H/C–C activation, *Org. Chem. Front.*, 2022, **9**, 1056–1064.

39 Z.-H. Wu and D.-C. Fang, DFT Study on Ruthenium-Catalyzed N-methylbenzamide-Directed 1,4-Addition of the Ortho C–H Bond to Maleimide *via* C–H/C–C Activation, *Org. Chem. Front.*, 2022, **9**, 6808–6816.

40 X.-R. Zhu and D.-C. Fang, DFT study on stereoselective Rh-catalyzed intramolecular [2+2+2] cycloaddition of allene-ene-ynes, *Org. Chem. Front.*, 2023, **10**, 2624–2634.

41 B. Lian, L. Zhang and D. C. Fang, A computational study on ruthenium-catalyzed [4+1] annulation *via* C–H activation: the origin of selectivity and the role of the internal oxidizing group, *Org. Chem. Front.*, 2019, **6**, 2600–2606.

42 L. Zhang, L.-L. Wang and D.-C. Fang, DFT Case Study on the Comparison of Ruthenium-Catalyzed C–H Allylation, C–H Alkenylation, and Hydroarylation, *ACS Omega*, 2022, **7**, 6133–6141.

43 B. Lian, L. Zhang, S.-J. Li, L.-L. Zhang and D.-C. Fang, Pd^{IV} Species Mediation in Pd^{II}-Catalyzed Direct Alkylation of Arenes with Oxiranes: A DFT Study, *J. Org. Chem.*, 2018, **83**, 3142–3148.

44 B. Lian, L. Zhang, G. A. Chass and D.-C. Fang, $Pd(OAc)_2$-Catalyzed C–H Activation/C–O Cyclization: Mechanism, Role of Oxidant—Probed by Density Functional Theory, *J. Org. Chem.*, 2013, **78**, 8376–8385.

45 D. C. Fang, *THERMO, Beijing Normal University, Beijing*, China, 2013.

46 J. Buaaa, J. Džurina, E. Hayryan, S. Hayryan, C.-K. Hu, J. Plavka, I. Pokorný, J. Skřivánek and M.-C. Wu, ARVO: A Fortran package for computing the solvent accessible surface area and the excluded volume of overlapping spheres *via* analytic equations, *Comput. Phys. Commun.*, 2005, **165**, 59–96.

47 R. F. W. Bader, *Atoms in Molecules*, Oxford University Press, USA, Oxford, 1994.

48 W.-H. Mu, G. A. Chasse and D.-C. Fang, Test and modification of the van der Waals' radii employed in the default PCM model, *Int. J. Quantum Chem.*, 2008, **108**, 1422–1434.

49 S. Kozuch and S. Shaik, How To Conceptualize Catalytic Cycles? The Energetic Span Model, *Acc. Chem. Res.*, 2011, **44**, 101–110.

50 S. Kozuch and S. Shaik, Combined Kinetic-Quantum Mechanical Model for Assessment of Catalytic Cycles: Application to Cross-Coupling and Heck Reactions, *J. Am. Chem. Soc.*, 2006, **128**, 3355–3365.

51 A. Uhe, S. Kozuch and S. Shaik, Automatic Analysis of Computed Catalytic Cycles, *J. Comput. Chem.*, 2011, **32**, 978–985.

